ON THE USE OF IW SENTINEL-1 SCENES FOR THE DETECTION AND MONITORING OF SURFACE MOTIONS IN THE RIACHO DOS MACHADOS GOLD MINE (SOUTHEASTERN BRAZIL)

Marcos Eduardo Hartwig - Federal University of Espirito Santo - marcos.hatwig@ufes.br
Leandro Ribes de Lima - Leagold Mining Company
Daniele Perissin - Purdue University

RESUMO

A interferometria de radar por espalhadores persistentes – PSI é uma técnica poderosa que combina imagens orbitais de radar no intuito de detectar e monitorar deslocamentos superficiais diminutos de vastas áreas. Nos últimos anos, o satélite Sentinel-1 produziu imagens do globo terrestre com diferentes resoluções espaciais e temporais que estão disponíveis gratuitamente. O objetivo deste trabalho é avaliar estas imagens no intuito de detectar e monitorar os deslocamentos na Mina de Au de Riacho dos Machados – MRDM (Estado de Minas Gerais, sudeste do Brasil). Os resultados mostraram que as imagens IW em modo descendente podem ser utilizadas para fornecer uma visão geral do estado de deformação ao longo da linha de visada do sensor - LOS. No intuito de monitorar a evolução do fenômeno deformacional induzido por mineração, mapas de deformação LOS poderiam ser gerados no mínimo a cada 12 dias.

Palavras-chave: Sensoriamento remoto por radar; Mina a céu aberto; PSI; Estabilidade de taludes.

ABSTRACT

The Persistent Scatterer Interferometry – PSI is a powerful technique, which combines radar satellite data in order to detect and monitor tiny surface displacements over vast areas. In the last years, the Sentinel-1 SAR mission have produced images of the globe acquired with different spatial and temporal resolutions that are freely available. The focus of this paper is to evaluate these scenes in order to detect and monitor surface displacements in the Riacho dos Machados Mine – MRDM (Minas Gerais state, southeastern Brazil). The results have shown that descending IW Sentinel-1 scenes can be used to provide a broad picture of the Line-Of-Sight - LOS deformation phenomena. In order to monitor the evolution of the deformation phenomena induced by mining activities, LOS deformation maps with millimeter accuracy could be only delivered at least each 12 days.

Keywords: Radar remote sensing; Open pit mine; PSI; Slope stability.

INTRODUCTION

Mining activities inevitably induce surface displacements. If they are not correctly detected and interpreted, they can overcome acceptable limits and eventually lead to failure, affecting production, safety of workers, mining equipment, etc. In order to avoid such a problem, in situ geotechnical monitoring systems are commonly employed, such as optical leveling, GPS, ground-based radar interferometry, extensometer, etc. Nevertheless, these methods are used only after the detection of geotechnical problems by field inspection, such as terrain cracks, rock/soil failures, sudden changes in the groundwater behavior, etc. Besides, traditional geotechnical monitoring systems can provide only punctual information about the deformation state.

In order to anticipate risk situations in mining activities, remote sensing techniques such as the Persistent Scatterer Interferometry - PSI have increasingly been used in the last decade ([1]; [2]; [3]; [4]). This satellite-based approach allows detecting and monitoring tiny surface displacements over large areas with millimetric to centimetric accuracy, day and night, independently of the weather conditions. The PSI method consists in combining large sets of complex synthetic aperture radar (SAR) scenes, obtained from different positions both in space and time. This approach exploits the phase differences of the signals of ground targets that exhibit high temporal phase stability, also called persistent scatterers - PS. Since the phase of the electromagnetic wave depends on the distance between the antenna and the target, it is possible to track superficial displacements over time.

For geotechnical applications, satellite scenes with high spatial and temporal resolutions are usually required, which can only be achieved by using commercial satellite data. In 2014 and 2016 the European Space Agency – ESA launched the Sentinel-1 constellation of two satellites. The Sentinel-1 is a C-band synthetic aperture-imaging mission developed for land monitoring. The satellites acquire images globally in different modes with temporal frequency of 6 and 12 days. The interferometric wide swath mode (IW) are freely available and have 5 x 20 meters spatial resolution. These characteristics make IW Sentinel-1 data suitable for many different applications, particularly large-scale deformation phenomena ([5]; [6]; [7]; [8]).

The Riacho dos Machados Gold Mine (MRDM) is located in the northeastern portion of the Minas Gerais State and comprises an open pit mine with almost 100 meters of depth, mined in decomposed greenish schists oriented NNE-SSW. The mineralization is hosted in paleoproterozoic quartz-muscovite-schists, affected by ductile-brittle shear zones and hydrothermalism developed during the Brazilian Tectonic Cycle (Neoproterozoic) ([9]). The MRDM has mineral reserves estimated in 3 million of tons with average Au grade of 0.94 g/t. In 2016, the mine was acquired by Brio Gold Mining Company which was purchased by the Leagold Mining Company in 2018. From May 2016 to May 2018, 102,283 oz of gold was produced in the MRDM ([10]).

In recent years, the Central and South pits of the MRDM have been recording planar failures (both global and local) in the footwall slopes controlled by the metamorphic foliation planes, which eventually interrupted ore exploitation in 2015. In 2017, a new smaller rock failure occurred in the footwall slopes of the South pit ([11]). In this sense, the aim of this work is to evaluate the applicability of the freely available IW Sentinel-1 SAR scenes in order to detect and monitor surface displacements induced by mining activities. For this purpose, 39 complex radar scenes acquired in descending orbit track between January 2018 and April 2019 were interferometrically processed in the SARPROZ software. The results were inspected in the field and compared to in situ and real-time geotechnical monitoring data.

STUDY AREA

Site geology and geomechanical conditions

The MRDM is included in a granitic-gneissic and migmatitic Archean basement window, termed as Guanambi-Correntina block (or Porteirinha Complex). This tectonic block is enveloped by Proterozoic metassedimentary rocks of the Serra do Espinhaço Thurst Belt, developed because of the Araçuaí-West Congo Orogen ([12]). Over the Guanambi-Correntina block outcrops a sequence of Paleoproterozoic/Archean metavolcanic-sedimentary rocks designated as Riacho dos Machados Group (GRM). In the mine area, the GRM comprises a sequence of sheared and hydrotermalized quartz-muscovite schist, quartz-feldspar schist and pelitic schist oriented N20°E. Gold mineralization is mainly hosted in the quartz-muscovite schists (QMX) and is related with the content of sulfides (arsenopyrite) ([9]).

The most penetrative geological structure observed in the mine area is an undulating schistosity oriented 113/45° (dip direction/dip convention). Brittle geological structures such as joints show a significant range of orientations and are observed throughout the mine area ([13]). According to the technical report of [13], rock mass in the mine area shows increasing values of strength with depth. The report identify four classes of rock mass quality ([14]) distributed horizontally throughout the mine (Figure 1). The rock mass quality tends to increase with depth.

Climate and weather conditions

According to [15] the region shows a Koppen-Geiger climate type Aw, that is, tropical weather with dry winter. Climate can be grouped in cold and hot seasons. Cold season usually ranges from October to March and hot season comprises all the other months. The study area can be subjected to extreme weather conditions according to [10]. In January 2014, a rainfall of 680 mm in one single storm event was recorded. From 2015 to 2017 the mine experienced an intense drought, which has affected water supply and ore production. Daily precipitation for the study area during the period of acquisitions of the Sentinel-1 SAR scenes shows that total precipitation for the entire period is 883 mm. Maximum precipitation reached 95 mm in 2018/04/02. Only the scene acquired in 2018/11/06 was affected by rain and precipitation is 36.3 mm.

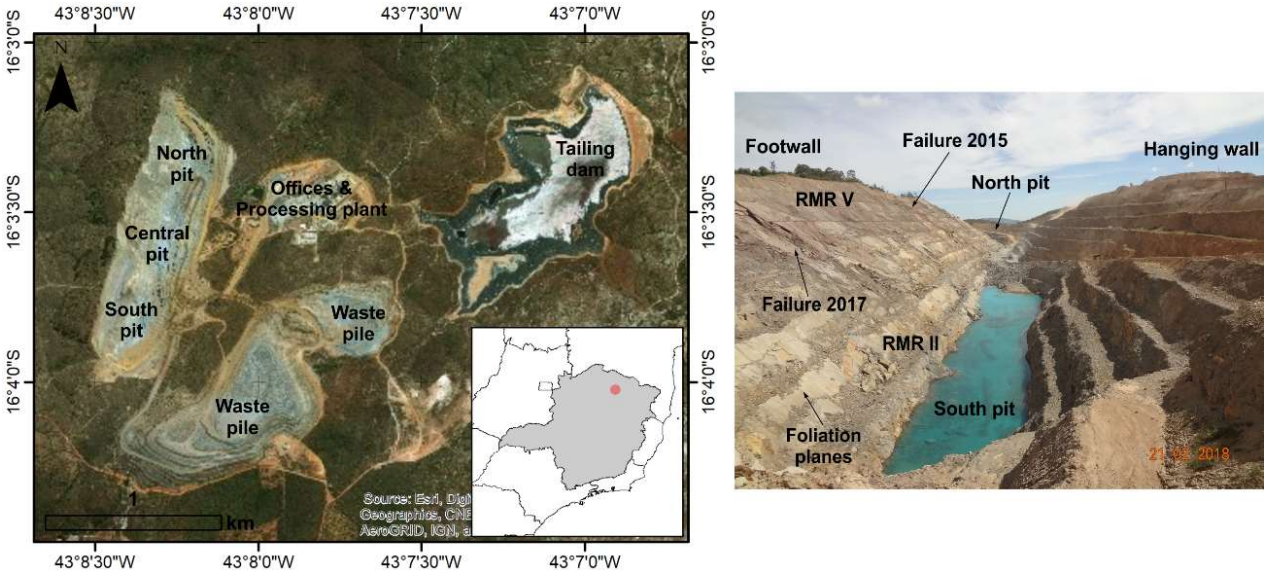

Figure 1. Location of the study area (left) and overview of the mine with indication of past failures and RMR (Rock Mass Rating) geomechanical classes (right).

SAR, DINSAR AND PSI OVERVIEW

Radar remote sensing comprises active systems that present lateral viewing geometry, which may lead to image distortions, particularly if it is acquired over rugged terrains (e.g., layover, foreshortening and shadow). Synthetic Aperture Radar – SAR transmits polarized electromagnetic waves within microwave frequencies (electromagnetic wavelength, λ = 1-100 cm) and record as a complex number, the amplitude and phase signal backscattered from ground targets for each resolution cell of an illuminated scene. The amplitude of the backscattered signal represents the reflectivity of the targets and depends on target and system parameters (e.g., dielectric constant, roughness, etc.). The phase of the signal indicates the cycle stage in which the wave is at a given moment. This angular quantity varies from 0 to 2π radians ([16]).

SAR interferometry (or simply InSAR) consists of combining two co-registered complex scenes, acquired from slightly different positions in space and time, along or across orbit track, to form an interferometric pair ([17]; [18]) (Figure 2). The spatial and temporal separation of the acquisitions are called normal and temporal baselines, respectively. The interferometric phase difference ($\Delta\phi$) can be derived by multiplying a master scene (reference) by the complex conjugated of a slave scene. This quantity will depend on the sensor-target distance (Δr) as follows:

$$\Delta\phi = \phi_1 - \phi_2 = \frac{2(2\pi)}{\lambda}(r_1 - r_2) \quad \text{(Eq. 1)}$$

The value 2 in the equation above refers to the round-trip of the radar signal.

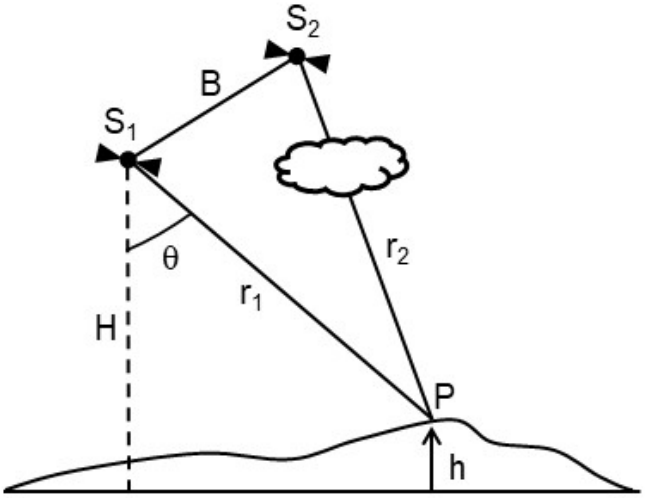

Figure 2. InSAR geometry. S1 and S2 correspond to the positions of the antennas in different acquisition times. B is the spatial separation of the antennas, θ is the view angle of the sensor, H is the height of the satellite, r corresponds to the slant range distance and h is the terrain height in the point P with respect to a reference surface (horizontal line).

Since the SAR scenes are usually acquired in different spatial and temporal positions, the interferometric phase difference will contain contributions from different sources:

$$\Delta\phi = \phi_{deformation} + \phi_{\boldsymbol{topography}} + \phi_{atmosphere} + \phi_{noise} + \phi_{orbit} \quad \text{(Eq. 2)}$$

The so-called Differential Synthetic Aperture Radar Interferometry - DInSAR technique consists of isolating the deformation component of the phase from the others ([19]; [20]; [21]). However, in spite of its centimetric accuracy ([22]), the DInSAR technique can be severely affected by atmospheric delay ([23]). In order to tackle with this issue, [24] and [25] originally patented the Persistent Scatterer Interferometry – PSI. The PSI consists of a multi-temporal analysis of the phase stability of stable scatterers across large stacks of SAR scenes. It was recognized that rock outcrops and man-made structures show a stable behavior over long periods of time and thus exhibit high temporal coherence. Because of the reflection dominance and consistency of these point-like scatterers within the resolution cell over time, the uncorrelated atmospheric phase component can be estimated and removed from each interferogram. In the PSI approach all SAR scenes are processed at full spatial resolution scale and connected to a unique master scene. The selection of the master scene is based on the spatial and temporal baselines of the dataset (the best combination of the scenes that results in the highest temporal coherence). Due to phase ambiguities, that is, sudden phase changes either in space or in time, a linear model is assumed in order to derive deformation rates. Deformation rates are then computed with respect to a stable reference point selected within the imaged scene, since phase differences are relative both in space and time.

Currently, there is a large number of PSI methods, also called Advanced DInSAR (A-DInSAR). These methods can be distinguished based on the baseline configuration, image resolution, ambiguity resolution method, a-priori pixel selection, a-posteriori pixel selection and atmospheric signal estimation ([26]; [27]; [28]; [29]; [30]). A review about the PSI methods and principles can be found in [31] and [32].

The PSI methods can be subjected to decorrelation effects due to physical and geometrical changes of the surface, such as moisture, erosion, volcanic episodes, rain, etc. These can lead to phase degradation, which limits the applicability of the method. In order to achieve deformation measurements within millimetric accuracy, at least 25-30 SAR scenes are usually interferometrically processed ([33]). The maximum detectable surface displacements will depend on the radar wavelength, the temporal and spatial resolutions, rate and type of deformation (e.g., smooth versus abrupt surface motions) and the spatial scale of the deformation phenomena. According to [32], [34] and [35] the theoretical maximum detectable displacement between acquisitions and between adjacent pixels is $\lambda/4$, where lambda is the radar wavelength. Another aspect involved with this technique is that it can only measure a one-dimensional motion along the line-of-sight (LOS) of the sensor (Figure 3). In order to retrieve vertical and horizontal displacements, data acquired in both ascending and descending passes must be geometrically combined ([36]).

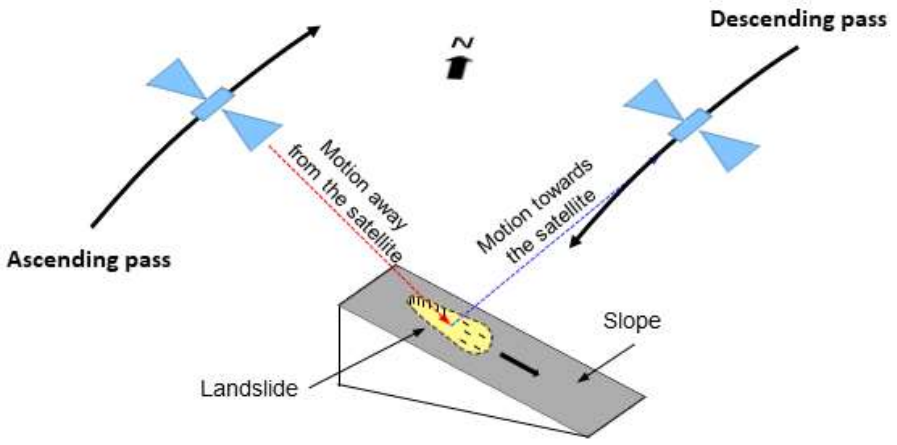

Figure 3 - Measurable surface displacement in ascending and descending geometries. Displacements along the orbit track cannot be detected.

THE SATELLITE SENTINEL-1

The Sentinel-1 constellation of two satellites is a global radar-imaging mission developed by the European Space Agency – ESA. The Sentinel-1A was launched in 2014 and the Sentinel-1B in 2016. The single look complex – SLC scenes are freely available at https://sentinel.esa.int/web/sentinel/sentinel-data-access. Table 1 summarizes the main features of the Sentinel-1 satellites.

The satellites operate in four acquisition modes: Stripmap (SM), Interferometric Wide swath (IW), Extra-Wide swath (EW) and Wave (WV). The IW mode acquires data with 250 km swath at 5 x 20 meter spatial resolution. IW mode captures three sub-swaths by using the TOPSAR technique. As a result, IW SLC products contain one image per sub-swath. Each sub-swath image consists of a set of bursts, each of them are processed as a single SLC image and between sub-swaths and adjacent bursts there are black-fill demarcation stripes.

In Brazil, Sentinel-1 imagery has been acquired since 2015 and is only available in descending mode each 12 days.

Table 1. Main features of the Sentinel-1 satellites.

Orbit	near-polar, sun-synchronous
Polarization	HH+HV; VV+VH; VV; HH
Revisiting time	12 days (6 days with both satellites)
Incidence angle	20 - 46 degrees
Altitude	693 km
Inclination	98.18 degrees
Frequency	5.405 GHz (λ = 5.54 cm | C-band)

DATASET AND METHODS

In this study, we used 39 SLCs descending scenes from the Sentinel-1B satellite, in VV polarization, acquired in the interferometric wide swath mode – IW (sub-swath 3) from 2018/01/10 to 2019/04/11 (16 months), with incidence angle range of 41 to 53 degrees (45 degrees in the study area). These images were processed in the SARPROZ software (https://www.sarproz.com/). The Persistent Scatterer Interferometry - PSI method was applied. In order to minimize temporal baseline and maximize temporal coherence, the scene acquired at 2018/09/19 was chosen as the master scene for the generation of the interferograms. Perpendicular baselines are below to ±104 meters. For the compensation of the topographic effects, the SRTM DEM (30m) was used. A stable reference point with high temporal coherence, outside the mining area was selected for the estimation of the deformation rates. The processing chain is summarized in Figure 4.

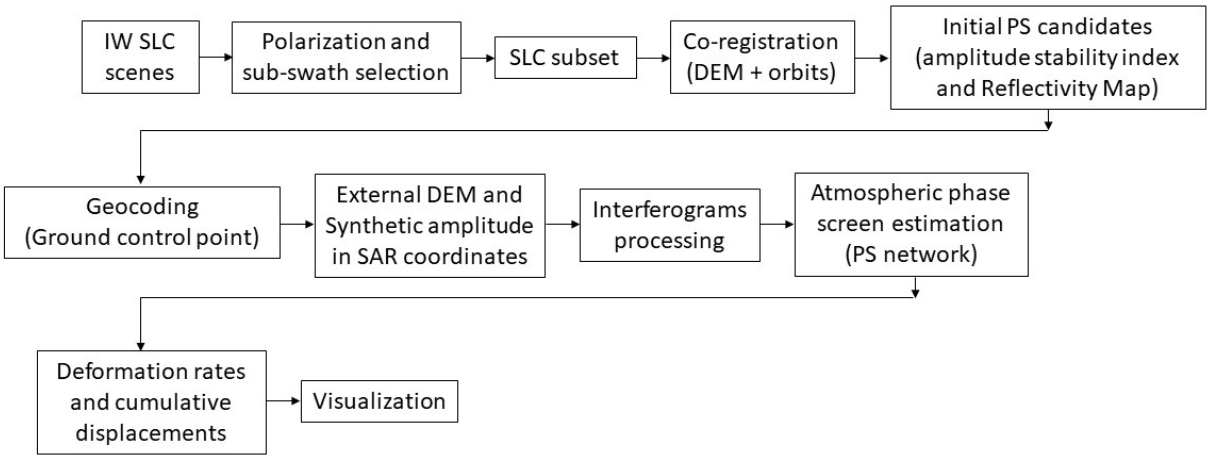

Figure 4. SARPROZ workflow for multi-temporal InSAR.

Validation with in-situ measurements is not trivial due to non-identical measurements locations in both space and time and non-identical reference points. Nevertheless, in order to validate the deformation time series measured from space, we tentatively compared it with vertical displacements measured through Total Station Leveling ([37]). This method can determine the full 3D displacement vector. For this study, only one benchmark prism was available (Figure 5) and displacements were recorded from 2018/01/03 to 2018/04/27. Prism accuracy is about two millimeter. Sentinel-1 SAR scenes were acquired approximately at 05h19a.m each 12 days. Therefore, we compare the closest data in both space and time. The spatial distance between the PS and the benchmark is 25 m. Since InSAR can provide only the component of the deformation along the line of sight, in order to keep results comparable, we multiplied the benchmark measurements by the cosine of the local incidence angle ([1]).

As stated in Item 3, radar scenes may be subjected to geometric distortions, such as layover, foreshortening, etc., due to slope orientation (aspect) and slope inclination with respect to the radar incidence angle of illumination. These effects when present in a complex radar scene make phase information useless. Sentinel-1 exhibits very low sensitivity for motion detection for slopes with displacement vectors parallel to its orbit track. In the study area, this corresponds to NNE and SSW-facing slopes. Issues as described above can be minimized by using radar scenes with different incidence angle or by combining radar scenes acquired in ascending and descending orbit tracks ([36]).

RESULTS AND DISCUSSIONS

In mining activities, surface displacements may be induced in three main different ways: 1) due to underground and slope excavations; 2) due to mining waste disposal in waste piles; and 3) due to discarding of mining byproducts after ore concentration in tailings dams. [38] and [39] pointed out many reasons for that, such as poor rock mass quality, induced vibrations, poor rock blasting, inadequate slope geometry (both height and slope angle), slope erosion, lithologies with reduced strength, high rock stress, unfavorable geological structures (both orientation and strength properties), high underground water pressures, etc.

The acceptable amount of (absolute and rate) of displacements depends overall on the strength and deformability properties of rock masses and earth-like materials ([40]). Displacement warning levels are defined then usually as low, moderate and high and are updated as new data is compiled during mine life span. When a warning level is reached, a set of procedures is immediately implemented in order to keep geotechnical risks acceptable.

Figure 5 depicts LOS deformation map for the entire MRDM for the period between January 2018 to April 2019. A total of 630 PS was detected over the processed area, which corresponds approximately to 45 PS/km2. PS are distributed heterogeneously over the area. Cumulative displacements range from -16,9 to +7,7 mm. Displacement accuracy varied between 1.4 to 7.9 mm. The deformation state does not shows critical behavior, considering the deformation magnitudes observed in the period and the warning levels adopted for mining operation (slope displacement below 50 mm is considered normal for open pit mining operation). In addition, no anomalous behavior have been reported elsewhere in the mine area during the image acquisition interval. Data shows a gentle subsidence pattern over waste piles and over the footwall slopes of the North and Central pits. [2] and [41] have described displacements well above these results for the waste piles of the N4 iron mines, Amazon region (deformation rates over -20 cm/year). [1] detected deformation rates over waste piles in the Azul Mn Mine equal to -17 cm/year.

PS was not detected in areas with low temporal coherence. That is, vegetated areas, excavated surfaces, water bodies, etc.

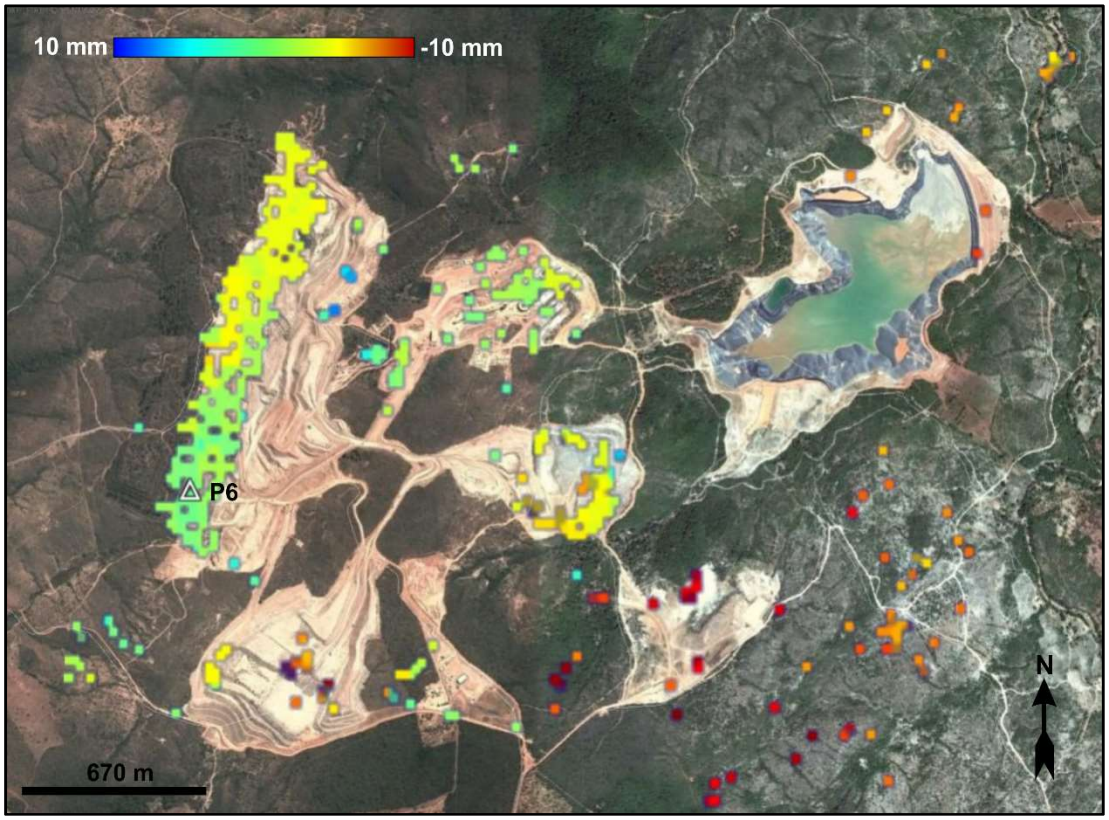

Figure 5. LOS deformation map for the entire MRDM overlaid on GoogleEarth optical imagery for the period from January 2018 to April 2019. Open triangle represents the benchmark prism used for validation purposes.

PSI VALIDATION

Figure 6 compares displacements obtained by benchmark prism P6 and PS463. Considering the fact that data was not recorded exactly in the same place and time and the accuracy of both instruments, it can be stated that displacements are in reasonable agreement. Moreover, displacements do not show any clear tendency and their magnitudes are small, indicating that the slope can be considered stable for this period.

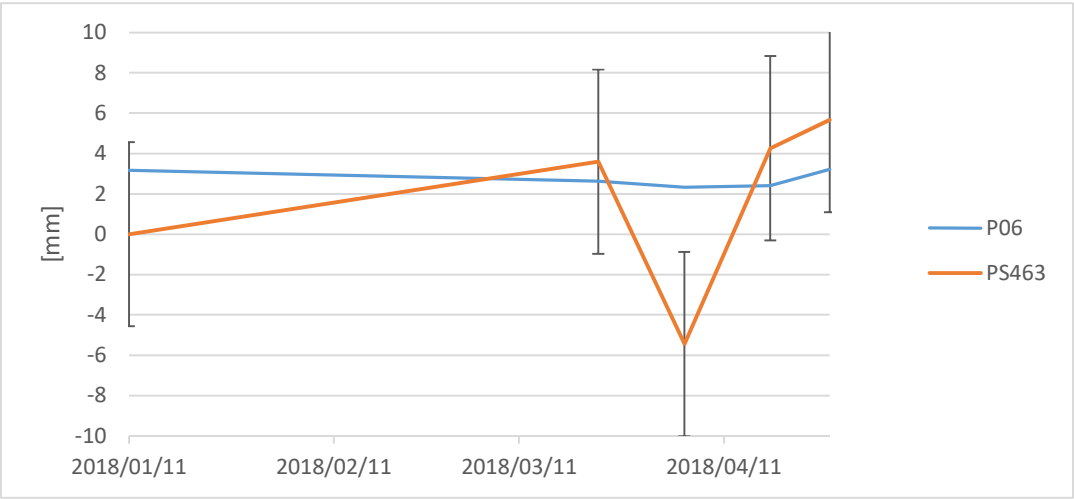

Figure 6. Validation of surface deformation measured from space.

FINAL REMARKS AND OUTLOOK

This work aimed to evaluate the applicability of the freely available Sentinel-1 SAR scenes for detecting and monitoring mine-induced displacements based on the PSI technique for the MRDM. The following can be stated:

1) Small values of deformation (< |16.9| mm) have been remotely detected for the MRDM. That indicates an stable geotechnical behavior considering the expected deformation levels for mining operation;
2) Sentinel-1 IW SAR scenes can be used to provide a broad picture of the LOS deformation phenomena induced by mining activities, indicating areas that demand critical monitoring;
3) Deformation maps based on Sentinel-1 SAR scenes should be combined with data derived from other monitoring methods as well as with regular field inspections. The PSI method based on only one SAR acquisition geometry can retrieve only the component of displacement along the line of sight of the antenna. Moreover, motions along orbit track are not detectable by this method;
4) Deformation maps with millimeter accuracy based only on descending Sentinel-1 SAR scenes can be produced each 12 days since the processed data set is large enough (one year of data acquisition or more). The amount of SAR data depends also on the deformation pattern in the area. Sites subjected to strong non-linear deformation must be assessed on a case by case basis.

REFERENCES

[1] PINTO, C. A.; PARADELLA, W. R.; MURA, J. C.; GAMA, F. F.; SANTOS, A. R.; SILVA, G. G.; HARTWIG, M. E. (2015). Applying persistent scatterer interferometry for surface displacement mapping in the Azul open pit manganese mine (Amazon region) with TerraSAR-X StripMap data. J. Appl. Rem. Sens. 9(1) 095978. 22 of December 2015.

[2] HARTWIG, M. E. (2016). Detection of mine slope motions in Brazil as revealed by satellite radar interferograms. Bulletin of Engineering Geology and the Environment. v. 75. p. 605-621.

[3] HARTWIG, M.; PARADELLA, W.; MURA, J. (2013). Detection and Monitoring of Surface Motions in Active Open Pit Iron Mine in the Amazon Region, Using Persistent Scatterer Interferometry with TerraSAR-X Satellite Data. Remote Sensing. v. 5. p. 4719-4734.

[4] COLESANTI, C.; WASOWSKI, J. (2006). Investigating landslides with space-borne Synthetic Aperture Radar (SAR) interferometry. Engineering geology, v.88. p. 173-199.

[5] FUNNING, G.; GARCIA, A. (2019). A systematic study of earthquake detectability using Sentinel-1 Interferometric Wide-Swath data. Geophysical Journal International. v. 216, Issue 1, p. 332–349. https://doi.org/10.1093/gji/ggy426

[6] INTRIERI, E.; RASPINI, F.; FUMAGALLI, A.; PING LU; CONDE, S.; FARINA, P.; ALLIEVI, J.; FERRETTI, A.; CASAGLI, N. (2018). The Maoxian landslide as seen from space: detecting precursors of failure with Sentinel-1 data. Landslides. v.15. p. 123-133. https://doi.org/10.1007/s10346-017-0915-7.

[7] SOWTER, A.; AMAT, M.B.C.; CIGNA, F.; MARSH, S.; ATHAB, A.; ALSHAMMARI, L. (2016). Mexico city land subsidence in 2014 – 2015 with Sentinel-1 IW TOPS: results using the Intermittent SBAS (ISBAS) technique. Int. J. Appl. Earth Obs. Geoinf. v. 52. p. 230-242.

[8] NAGLER, T.; ROTT, H.; HETZENECKER, M.; POTIN, W.P. (2015). The Sentinel-1 Mission: New Opportunities for Ice Sheet Observations. Remote Sensing. v. 7. n. 7. p. 9371-9389.

[9] FONSECA, E. (1993). Depósito aurífero de Riacho dos Machados, norte de Minas Gerais: hidrotermalismo, deformação e mineralização associada. 179p. Dissertação (Mestrado em Geologia) – Instituto de Geociências, Universidade Federal de Minas Gerais, Belo Horizonte, Brasil.

[10] RPA INC. (2018). Technical report on the Riacho dos Machados Gold Mine, Minas Gerais, Brazil (NI 43-101 Report). Toronto: Relatório interno Brio Gold Inc.

[11] VOG. (2017). Estudos conceituais análise geotécnica para o push back – cava sul (Vog n° VG16-193-1-GL-RTE-0001). Belo Horizonte: Relatório interno Brio Gold Inc. 28p.

[12] ALKMIM, F.F.; MARSHAK, S.; PEDROSA-SOARES, A.C.; PERES, G.G.; CRUZ, S.C.P.; WHITTINGTON, A. (2006). Kinematic evolution of the Araçuaí-West Congo Orogen in and Africa: nutcracker during the Neoproterozoic assembly of Gondwana. Precambrian Research, v. 149, p. 43-64.

[13] GEOESTÁVEL. (2015). Estudos talude de cava final e recuperação talude de footwall – Mineração Riacho dos Machados (N° GSTCPT0001-01-1-GT-RET-0001_1). Belo Horizonte: Relatório interno Carpathian Gold inc. 441p.

[14] BIENIAWSKI, Z.T. (1989). Engineering rock mass classification. New York: John Wiley and Sons. 251p.

[15] REBOITA, M.S.; RODRIGUES, M.; SILVA, L.F.; ALVES, M.A. (2015). Aspectos climáticos do Estado de Minas Gerais. Revista Brasileira de Climatologia. v. 17. p. 206-226.

[16] MADSEN, S.N.; ZEBKER, H.A. (1998). Imaging radar interferometry. In: HENDERSON, F.M.; LEWIS, A.J. Principles & Applications of Imaging Radar – Manual of Remote Sensing, Third Edition, v. 2, Danvers, MA: John Wiley & Sons, Inc. p. 359-380.

[17] ROSEN, P.A.; HENSLEY, S.; JOUGHIN, I.R.; Li, F.K.; MADSEN, S.N.; RODRÍGUES, E.; GOLDSTEIN, R. (2000). Synthetic aperture radar interferometry. Proceedings of the IEEE, v. 88, n. 3, p. 333-382.

[18] BAMLER, R.; HARTL, P. (1998). Synthetic aperture radar interferometry. Inverse Problems. v. 14. p. R1-R54.

[19] AMELUNG, F.; GALLOWAY, D.L.; BELL, J.W.; ZEBKER, H.A.; LACZNIAK, R.J. (1999). Sensing the ups and downs of Las Vegas: InSAR reveals structural control of land subsidence and aquifer-system deformation. Geology, v. 27. n.6. p. 483-486.

[20] MASSONNET, D.; FEIGL, K.L. (1998). Radar interferometry and its application to changes in the Earth's surface. Reviews of Geophysics. v. 36(4). p. 441-500.

[21] CARNEC, C.; MASSONNET, D.; KING, C. (1996). Two examples of the use of SAR interferometry on displacement fields of small spatial extent. Geophysical Research Letters, v. 23. n. 24, p. 3579-3582.

[22] STROZZI, T.; WEGMÜLLER, U.; TOSI, L.; BITELLI, G.; SPRECKELS, V. (2001). Land subsidence monitoring with differential SAR interferometry. Photogrammetric Engineering & Remote Sensing, v. 67. n.11. p. 1261-1270.

[23] ZEBKER, H., ROSEN, P.; HENSLEY, S. (1997). Atmospheric effects in interferometric synthetic aperture radar surface deformation and topographic maps. Journal of Geophysical Research, v. 102. n.4. p.7547-7563.

[24] FERRETTI, A.; PRATI, C.; ROCCA, F. (2001). Permanent Scatterers in SAR Interferometry. IEEE Transactions on Geoscience and Remote Sensing, v.39. n.1. p.8-19.

[25] FERRETTI, A.; PRATI, C.; ROCCA, F. (2000). Nonlinear subsidence rate estimation using permanent scatterers in Differential SAR Interferometry. IEEE Transactions on Geoscience and Remote Sensing, v. 38. n.5. p. 2202–2212.

[26] PERISSIN, D.; WANG, T. (2012). Repeat-pass SAR interferometry with partially coherent
targets. IEEE TGRS 50 (1), 271–280.

[27] FERRETTI, A.; FUMAGALLI, A.; NOVALI, F., PRATI, C.; ROCCA, F.; RUCCI, A. (2011). A new algorithm for processing interferometric data-stacks: SqueeSAR. IEEE TGRS 49 (9), 3460–3470.

[28] HOOPER, A.; ZEBKER, H.; SEGALL, P.; KAMPES, B. (2004). A new method for measuring deformation on volcanoes and other natural terrains using InSAR persistent scatterers. Geophys. Res. Lett. 31 (23).

[29] WERNER, C.; WEGMULLER, U.; STROZZI, T.; WIESMANN, A. (2003). Interferometric point target analysis for deformation mapping. In: IGARSS'03, 2003, Toulouse, France. Proceedings… Toulouse: IEEE, 2003. v. 7. p. 4362-4364.

[30] BERARDINO, P.; FORNARO, G.; LANARI, R.; SANSOSTI, E. (2002). A new algorithm for surface deformation monitoring based on small baseline differential SAR interferograms. IEEE TGRS 40 (11), 2375–2383.

[31] PEPE, A.; CALÒ, F. (2017). A review of interferometric synthetic aperture radar (InSAR) multi-track approaches for the retrieval of Earth's surface displacements. Applied Sciences. v. 7. n. 1264. p. 1-39.

[32] CROSSETTO, M.; MONSERRAT, O.; CUEVAS-GONZÁLES, M.; DEVANTHÉRY, N.; CRIPPA, B. (2016). Persistent Scatterer Interferometry: a review. ISPRS Journal of Photogrammetry and Remote Sensing. v. 115. p. 78-89.

[33] COLESANTI, C.; FERRETTI, A.; PRATI, C.; ROCCA, F. (2003). Monitoring landslides and tectonic motion with the Permanent Scatterers technique. Engineering Geology. v. 68. p. 3-14.

[34] WASOWSKI, J.; BOVENGA, F. (2014). Investigating landslides and unstable slopes with satellite Multi Temporal Interferometry: Current issues and future perspectives. Engineering Geology. v.174. p. 103-138.

[35] SABATER, J.R.; DURO, J.; ARNAUD, A.; ALBIOL, D.; KOUDOGBO, F.N. (2011). Comparative analyses of multi-frequency PSI ground deformation measurements. In: PROCEEDINGS OF THE INTERNATIONAL SOCIETY FOR OPTICAL ENGINEERING – SPIE, 2011. Prague, Czech Republic. 2011. Proceedings…Prague: SPIE. 2011. vol. 8179. p. 81790M - 81790-12M.

[36] FUHRMANN, T.; GARTHWAITE, M.C. (2019). Resolving Three-Dimensional Surface Motion with InSAR: Constraints from Multi-Geometry Data Fusion. Remote Sensing. v. 11. n.3. p. 1-21.

[37] COLESANTI, C.; FERRETTI, A.; PRATI, C.; ROCCA, F (2001). Comparing GPS, optical leveling and permanent scatterers. In: IGARSS, Sydney, Australia. Proceedings… Sydney: IEEE, 2001, v.6., p. 2622-2624.

[38] READ, J.; STACEY, P. (2009). Guidelines for open pit slope design. Leiden: CRC. 496p.

[39] SJÖBERG, J. (1996). Large scale slope stability in open pit mining – a review. Sweden: Lulea University of Technology - Division of Rock Mechanics. 215p. Technical Report.

[40] ZAVODNI, Z.M. (2000). Time-dependent movements of open-pit slopes. In: Hustrulid et al. (eds.). Slope stability in surface mining. Littleton: Society for Mining, Metallurgy and Exploration, Inc. (SME). p. 81-87.

[41] PARADELLA W. R.; FERRETTI, A.; MURA, J.C; COLOMBO, D.; GAMA, F. F.; TAMBURINI, A.; SANTOS, A.R.; NOVALI, F.; Galo, M.; CAMARGO, P. O.; Silva, A.Q.; SILVA, G.G.; SILVA, A.; GOMES, L.L. (2015). Mapping surface deformation in open pit iron mines of Carajás Province (Amazon Region) using an integrated SAR analysis. Engineering Geology. v. 193. p. 61-78.